

Dynamics of leading lamellae of living fibroblasts visualized by high-speed scanning probe microscopy

Kazushi Tamura · Takeomi Mizutani ·
Hisashi Haga · Kazushige Kawabata

Accepted: 21 September 2009 / Published online: 9 October 2009
© Springer-Verlag 2009

Abstract In this study, we aimed at improving the temporal resolution of scanning probe microscopy (SPM) for observing living cells by introducing soft cantilevers, low feedback-gain operations, and cantilever deflection imaging. We achieved visualization of the mechanical architecture in leading lamellae of living fibroblasts at a temporal resolution of around 10 s, which is higher than that of conventional contact-mode SPM. Time-lapse SPM could be used to monitor not only cytoskeletal dynamics but also the dynamics of numerous microgranules. Statistical analysis of microgranular motion revealed that the microgranules have superdiffusive behaviors and significant directional order of motion. We also found that the direction of their motion is correlated with the direction of growing actin stress fibers. The combination of SPM with fluorescence microscopy showed that vinculin, a component of cell-substratum adhesion sites, localizes at the microgranules. Our experimental data provides a new insight into the intracellular mechanical architecture and its structural dynamics, suggesting that high-speed live-cell SPM has great potential for investigating the structural origin of cellular dynamics.

Keywords SPM · Atomic force microscopy · Cytoskeleton · Lamella · Leading edge · Cell mechanics

Introduction

Scanning probe microscopy (SPM), also known as atomic force microscopy, is a powerful technique for investigating the structure and mechanics of biological components, because this method can be applied directly to image the topography of mechanical architecture in soft materials and measure mechanical forces quantitatively in liquid conditions. A topographic imaging application, such as contact-mode SPM, allows visualization of mechanical architectures in cells or tissues (Henderson et al. 1992; Raspanti et al. 2001; Habelitz et al. 2002; Pesen and Hoh 2005), whereas quantitative force measurement reveals the viscoelasticity of cells or tissues (Radmacher et al. 1996; Alcaraz et al. 2003; Goffin et al. 2006) and the adhesive force between molecules or cells (Baumgartner et al. 2000; Benoit et al. 2000; Helenius et al. 2008). SPM has also been applied to examine the active and dynamical behaviors of biological components. However, the typical temporal resolution in conventional contact-mode SPM is longer than 1 min (Hansma et al. 2006). Therefore, time-lapse contact-mode SPM is suitable for observing minute-scale dynamics, such as the morphological changes of epithelial cells (Schoenenberger and Hoh 1994). In brief, conventional contact-mode SPM excels in the observation of slow biological dynamics rather than fast dynamics.

Recently, two types of high-speed SP microscopes for topographic imaging, based on either a high-speed feedback system (Ando et al. 2001) or no feedback system (Picco et al. 2007), have been introduced; these SP microscopes can achieve a temporal resolution of <0.1 s

Electronic supplementary material The online version of this article (doi:10.1007/s00418-009-0644-7) contains supplementary material, which is available to authorized users.

K. Tamura (✉) · T. Mizutani · H. Haga · K. Kawabata
Division of Biological Sciences, Graduate School of Science,
Hokkaido University, Kita 10, Nishi 8, Kita-ku,
Sapporo 060-0810, Japan
e-mail: tam@mail.sci.hokudai.ac.jp

even in liquid conditions. They have been used to visualize various biological components *in vitro*, such as motor proteins (Ando et al. 2001), collagen fibrils (Picco et al. 2007), and chromosomes (Picco et al. 2008). However, as both types of microscopes likely apply large frictional and compressive forces on samples, their application for visualizing living cells with soft and highly undulating surfaces seems difficult. A method allowing modulation of the applied forces is likely required for high-speed SP microscopic observation of the fast dynamics of biological components under physiological conditions.

Leading lamellae, the broad and thin peripheries of motile cells, are difficult but worthwhile to observe using SPM. The mechanical architecture in leading lamellae shows fast dynamics and produces drastic morphological changes of these lamellae, such as expansion, contraction, and ruffling. It is well known that the actin cytoskeleton is a main component of such mechanical architecture and plays a critical role in morphological regulation of leading lamellae: the elongation of filamentous actin (F-actin), induced by polymerization, elicits protrusions of the plasma membrane at the edge; the centripetal movement of F-actin networks, driven by molecular motor myosin II, results in retraction of the edge. Accompanied by the centripetal movement, F-actin is bundled into thick cables, called actin stress fibers (SFs). Recently, specific molecular interactions originating in these processes of actin cytoskeletal reorganization have been investigated. However, the comprehensive structural dynamics of such mechanical architecture is still poorly understood; there might be as-yet-unrecognized features of the overall mechanical architecture. High-speed live-cell SPM could reveal more comprehensive structural dynamics of this mechanical architecture.

In this study, to advance the application of SPM for observing the fast dynamics of living cells, we combined soft cantilevers to modulate the force applied to cells, low feedback-gain operations of a commercial SP microscope, and imaging of cantilever deflection. We achieved live-cell imaging of the mechanical architecture in leading lamellae with a temporal resolution of about 10 s. Time-lapse observations of the lamellae showed not only drastic remodeling of the actin cytoskeleton but also granular matter, which showed retrograde movement and minute-scale lifetimes. The number of granules decreased and their direction of movement correlated with the alignment of newly assembled SFs. Therefore, the dynamical behaviors of the mechanical architecture in leading lamellae were revealed for the first time using high-speed live-cell SPM. Combination of SPM with fluorescence microscopy showed that a part of the granular matter included vinculin, a terminal component of SFs. Our observations provided a new insight into the dynamics of the mechanical architecture in leading lamellae.

Materials and methods

Cell culture

Mouse embryonic fibroblasts (NIH-3T3; RIKEN Cell Bank, Tsukuba, Japan) were cultured in Dulbecco's modified Eagle's medium (DMEM; Invitrogen, Carlsbad, CA) with 10% heat-inactivated bovine serum (Invitrogen) and 1% antibiotic solution (Sigma-Aldrich, St. Louis, MO) at 37°C in a 5% CO₂ atmosphere. Trypsinized cells were spouted onto a chambered glass coverslip; a relatively low cell density was used to prevent intercellular contacts. After overnight culture, the medium was replaced with 4-(2-hydroxyethyl)-1-piperazineethanesulfonic acid (HEPES)-buffered DMEM (pH 7.4; Sigma-Aldrich) with 10% heat-inactivated bovine serum and 1% antibiotic solution for the measurements with SPM. The cells showed random migration because we did not apply a serum concentration gradient or chemical attractant to control cell migration. For these experiments, we used the extending lamellae of the cells.

SPM

The measurements were based on a commercial SP microscope (BioScope NanoScope IIIa; Veeco, Woodbury, NY), located in a thermally insulating box with a control unit for atmospheric temperature. The temperature-controlled microscope was combined with an inverse optical microscope (Eclipse TE2000-U; Nikon, Tokyo, Japan) on a vibration isolator. The sample temperature was controlled at $36 \pm 1^\circ\text{C}$.

We introduced the following procedures to achieve high temporal resolution. In typical contact-mode imaging, it is difficult to determine the topography of samples with highly undulating surfaces at high temporal resolution because the cantilever easily oscillates in response to the electronic feedbacks from the SP microscopic control unit. On the other hand, when the feedback is delayed, it is possible to visualize the topography by measuring cantilever deflection. This operation mode is called "error mode," because the deflection in contact-mode means the error in maintenance of constant deflection. In error-mode SPM (E-SPM), the cantilever height is kept almost constant, but cantilever deflection changes depending on the surface morphology of the samples (Fig. S1). We set the integral gain at 0.050, proportional gain at 0.050, and line scan rate at 10.2 or 15.3 Hz. We also set the number of lines in an image to 128. E-SPM has often been used for rigid and undeformable samples but not for cells because a cantilever may push the cell surfaces more strongly in error mode than in contact mode. To reduce cell damage, we controlled the force applied to cells to <1 nN by adjusting

the cantilever height. To improve the contrast of the images obtained using E-SPM, we used relatively soft cantilevers with a spring constant of 0.01 N/m (MLCT-AUHW; Veeco). Therefore, the inner architecture could be visualized with good contrast. Using these procedures, we achieved a temporal resolution of about 10 s without serious cell damage (e.g., cell death or membrane breakage). In this study, we used a temporal resolution of 12.6 s (line scan rate 10.2 Hz) or 8.4 s (line scan rate 15.3 Hz). The acquired images were filtered with a plane-fit. To reduce noise in some images, we finally filtered the images with an appropriate Fourier mask using Image-Pro (Media Cybernetics, Silver Spring, MD).

During SP microscopic observation, we captured optical microscopic images of the observed cells and the surrounding cells in order to identify the observed cells under the fluorescence microscopy system.

Fluorescence microscopy

Cells were fixed with 3.7% formaldehyde in phosphate-buffered saline (PBS) for 10 min, permeabilized with 0.5% Triton-X100 in PBS for 20 min, and incubated in PBS containing 0.5% bovine serum albumin (BSA) for 30 min prior to the reaction with antibodies. The cells were stained with mouse anti- α -tubulin antibody (1:500; Sigma-Aldrich), rabbit anti-myosin-IIA antibody (1:100; gift from Dr. Masayuki Takahashi, Hokkaido University, Sapporo, Japan), or mouse anti-vinculin antibody (1:2,500; Sigma-Aldrich) for 60 min followed by a mixed solution of MFP488-conjugated phalloidin (1:500; Mo Bi Tec, Göttingen, Germany) and secondary antibody for 60 min. The secondary antibody was Alexa546-conjugated goat anti-mouse IgG antibody (1:500; Invitrogen), for the mouse primary antibodies, or HiLyte555-conjugated goat anti-rabbit IgG antibody (1:200; AnaSpec, San Jose, CA), for the rabbit primary antibodies. All antibodies were diluted in PBS containing 0.5% BSA. After staining, we observed the fluorescent-stained cells using confocal laser scanning microscopy (CLSM, C1 confocal imaging system; Nikon). We were able to identify the cells observed using the SP microscope from the outline of the cells observed on optical microscopic images captured under the SPM system.

Movement tracking and statistical analysis

To analyze the two-dimensional movement of the granules observed using E-SPM, we manually measured x - y position $\mathbf{c}_i(j)$ of the i th single granule as a function of time-lapse frame number j from its appearance to disappearance in the observed window using Scion Image (Scion,

Frederick, MD). The time sequence, $\mathbf{c}_i(j)$, of a single granule gives its individual trajectories.

Displacement vector $\mathbf{d}_{i,\Delta j}(j)$ of the i th single granule at the j th frame with frame interval Δj was calculated as follows:

$$\mathbf{d}_{i,\Delta j}(j) = \mathbf{c}_i(j + \Delta j) - \mathbf{c}_i(j) \quad (1)$$

We then analyzed the mean-square displacement (MSD), of the i th single granule, calculated as follows:

$$\text{MSD}_{i,\Delta j} = \left\langle |\mathbf{d}_{i,\Delta j}(j)|^2 \right\rangle_j = \frac{1}{m} \sum_j |\mathbf{d}_{i,\Delta j}(j)|^2 \quad (2)$$

where m is the total number of $\mathbf{d}_{i,\Delta j}(j)$ at given i and Δj . We calculated the time interval, Δt , as Δj multiplied by the temporal resolution and calculated MSD at $\Delta j = 1, 2, 3, \dots, 10$.

To evaluate directional order and mean direction, we calculated normalized displacement vector $\mathbf{u}_i(j)$, as follows:

$$\mathbf{u}_i(j) = \frac{\mathbf{d}_{i,\Delta j}(j)}{|\mathbf{d}_{i,\Delta j}(j)|} \quad (3)$$

where $\Delta j = 2$. The mean vector, \mathbf{r} , of the normalized displacement vectors was introduced to evaluate the directional order and mean direction of $\mathbf{u}_i(j)$ statistically, as follows:

$$\mathbf{r} = \langle \mathbf{u}_i(j) \rangle_{i,j} = \frac{1}{n} \sum_i \sum_j \mathbf{u}_i(j) \quad (4)$$

where n is the total number of $\mathbf{u}_i(j)$. We defined directional order and mean direction as $|\mathbf{r}|$ and direction of \mathbf{r} , respectively. The $\mathbf{u}_i(j)$ orients randomly for $|\mathbf{r}| = 0$ and uniformly for $|\mathbf{r}| = 1$. To determine whether the calculated directional order is significantly different from 0, we applied Rayleigh's z test (Greenwood and Durand 1955; Zar 1999) to the data. We considered a P value of <0.001 as statistically significant.

Pharmacological treatment

To modulate the structure of actin cytoskeleton, we treated cells with cytochalasin-D or Y-27632. Cytochalasin-D inhibits actin polymerization and induces depolymerization of F-actin. Y-27632 specifically inhibits Rho-associated coiled-coil kinase (ROCK), which activates myosin regulatory light chain (MRLC). Dephosphorylation of MRLC induced by Y-27632 is known to disrupt SFs but not F-actin networks (Hirata et al. 2007). We prepared a Y-27632 solution at a concentration of 1 mg/ml and a cytochalasin-D solution at a concentration of 0.1 mg/ml. During the observation, we added these solutions to the cell culture media to a final concentration of 10 μM .

Results

Characterization of high-speed live-cell SPM

To confirm that E-SPM is superior for high-speed observation of living cells, we compared E-SPM with conventional contact-mode SPM by observing a lamella in a living fibroblast at a frame rate of 12.6 s/frame (Fig. 1). We set the field of view to 10 μm for observing both the near-cell edge and the near-cell body regions in the lamella simultaneously. In the case of the lowest feedback gain (corresponding to the observation condition on E-SPM), the deflection image clearly showed cytoskeletal filaments, although little signal was detected in the height image. With increased feedback gain (corresponding to the conventional contact mode), the oscillatory noise became stronger in both the deflection images and the height images. The height images did not clearly show cytoskeletal filaments. These results meant that the contact-mode SP microscope, showing height images based on feedback electronics, failed to monitor the mechanical architecture at the subminute-scale temporal resolution and that E-SPM was suitable for high-speed observation of living cells.

We estimated the tip indentation depth at the cell surfaces during high-speed observation by applying the procedures reported previously (Hertz 1882; Lavenberg 1944; Marquardt 1963; Haga et al. 2000; Tamura et al. 2007). The results have been described in the Supplementary Materials.

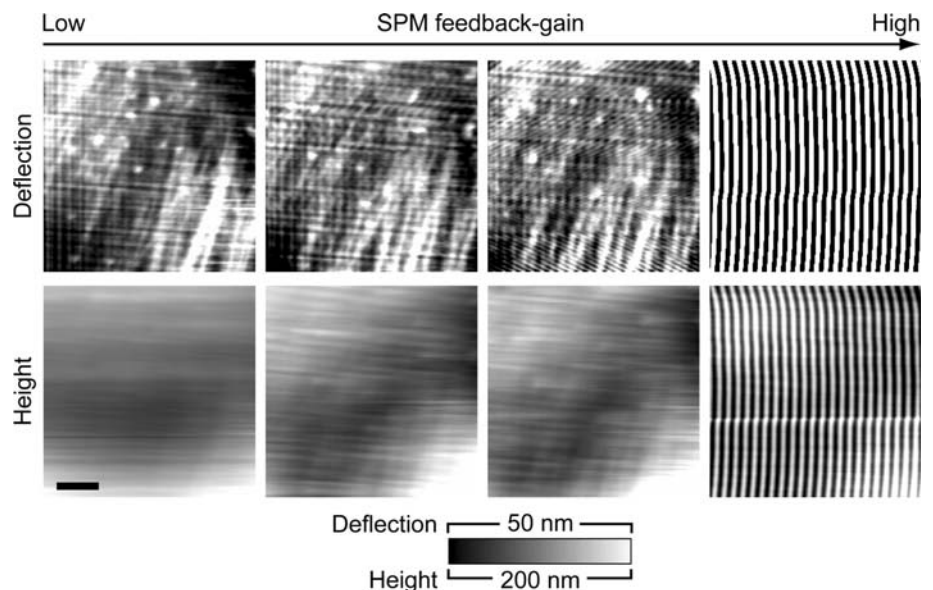
Dynamics of mechanical architecture

We succeeded in high-speed time-lapse observation of the lamellae in living fibroblasts using E-SPM. Obvious damage to cell morphology was not seen during our

observations. We obtained a typical time-lapse sequence of images with a frame rate of 12.6 s/frame (Fig. 2a, see also Supplemental Movie S1). In the images, we observed micrometer-sized granular matter embedded on filamentous networks. We named the granular matter “microgranules.” The microgranules appeared, moved, and then disappeared several minutes after their appearance. Simultaneously, thick cables of about 500 nm in diameter gradually emerged. The cables extended from the cell body toward the cell edge with a highly ordered alignment. The alignment feature of the cables was similar to SFs. We quantitatively analyzed time-dependent changes in the number of microgranules and length of the SF-like cables (Fig. 2b). The total number of microgranules in the image gradually decreased with time. Then, the SF-like cables gradually elongated. To further characterize the elongation dynamics of the SF-like cables (e.g., determination of elongation velocity), we analyzed time-dependent changes in the SP microscopic images during the formation of SF-like cables at subminute temporal resolution (Fig. 2c). The time-lapse sequence did not show continuous elongation of the SF-like cables. Hence, we could not define the elongation velocity in the subminute time scale. Instead, the sequence showed that the space surrounded by thin filaments gradually narrowed with time, and the thin filaments were finally bundled into a micrometer scale SF-like cable. The cable was assembled within approximately 2 min in a stepwise fashion. Similar observations were made eight times. Moving microgranules were observed in 6/8 cells. In the other two cells, microgranules were observed, but these were not motile. In 2/8 cells, we observed the emergence of new thick cables.

To examine whether the movement of the microgranules is based on a purely passive process (i.e., simple Brownian

Fig. 1 Changes in height and deflection images of a lamella of a living fibroblast depending on the increase of feedback gain. The lowest feedback gain was set to the same condition as for E-SPM. As the feedback gain was gradually increased, the oscillatory noise became stronger. Scale bar 2 μm



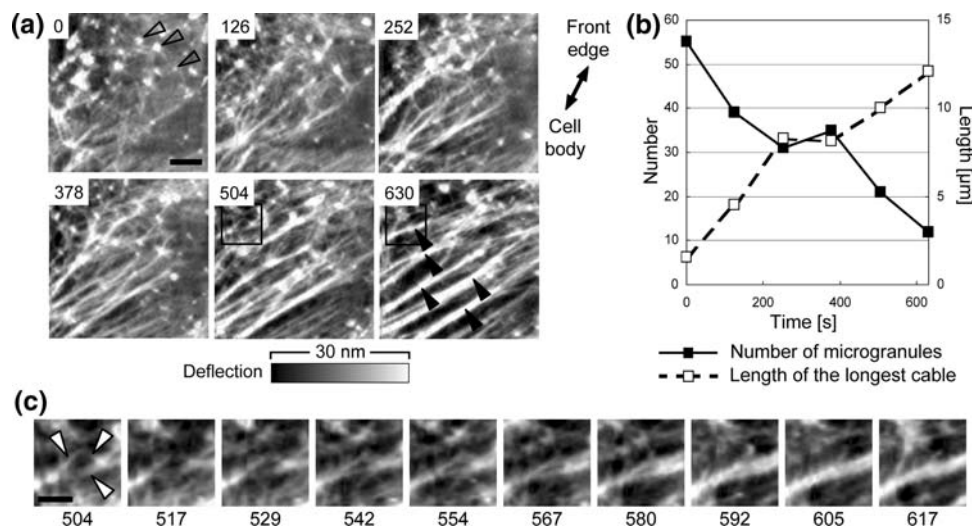


Fig. 2 Dynamics of microgranules and filamentous networks observed using time-lapse E-SPM. **a** Time-lapse images of a lamella of a living fibroblast obtained using E-SPM. Each image represents every tenth frame. The *open arrowheads* and *solid arrowheads* indicate typical microgranules and cables, respectively. The *number* in each image represents time in seconds. *Scale bar* 2 μm . **b** Number of microgranules and length of the longest cable within the images

obtained using E-SPM plotted as a function of time. The *solid squares* and *solid lines* indicate time-dependent change in the number of microgranules. The *open squares* and *dashed lines* indicate time-dependent change in the length of the longest cable. **c** Time-lapse E-SPM images at high temporal resolution in the area shown by the *square* in **a**. The *arrowheads* indicate thin filaments that are bundled into a cable. *Scale bar* 1 μm

diffusion) or not, we analyzed two-dimensional diffusion behavior of the microgranules by calculating the MSD. The trajectories of 11 microgranules are shown in Fig. 3a. The MSD of individual microgranules was plotted as a function of the time interval (Fig. 3b). The MSD– Δt curves fitted to the following power-law equation:

$$\text{MSD} = C(\Delta t)^\beta \quad (5)$$

where C is a constant. If the movement was a purely passive process, power exponent β should equal 1. Almost all the curves showed clear power-law behavior, and β was 1.19 ± 0.06 (mean \pm SE), indicating that the microgranules showed slightly but significantly faster diffusion than Brownian particles did (i.e., superdiffusion). To assess artifactual effects, such as hysteresis of the SP microscope and measurement noise, on microgranular MSD, we observed extracellular points and compared their MSD with the microgranular MSD. The MSD of the extracellular points was significantly smaller than that of the microgranules. Therefore, artifactual factors did not sufficiently affect the microgranular MSD. These findings meant that the microgranules showed superdiffusion and that active processes (e.g., ATP-dependent processes) might drive microgranules.

To investigate the spatial coordination of microgranular motion, we evaluated the directional order of their movement. Vector \mathbf{r} , the mean of normalized displacement vectors, was introduced and analyzed (Fig. 3c). The values of components of \mathbf{r} were -0.232 ± 0.034 for the x -axis and -0.082 ± 0.037 for the y -axis (mean \pm SE; calculated

for 376 vectors from 11 microgranules). Directional order, $|\mathbf{r}|$, was estimated to be 0.247. Applying Rayleigh's z test (Greenwood and Durand 1955; Zar, 1999) to the experimental $|\mathbf{r}|$, we confirmed that $|\mathbf{r}|$ was significantly larger than 0, with $P < 0.001$. The result indicated that the microgranular movement was oriented in a particular direction. In addition, the mean direction was toward the cell body. By comparing with trajectory maps (Fig. 3a) and the images obtained using E-SPM (Fig. 2a), we found that the microgranules moved along with the elongating SF-like cables. Here, we defined the range of the alignment angle of the SF-like cables by measuring their angle at 630 s (Fig. 3c). The mean direction of microgranular motion was in the range of the alignment angle. The result suggested that the movement orientation of the microgranules was based on a mechanism similar to the alignment of the SF-like cables.

Molecular compositions of mechanical architecture

To identify molecular compositions of the mechanical architecture (i.e., SF-like cables, filamentous networks, and microgranules), we fixed cells <1 min after observation using E-SPM and stained them with fluorescent-tagged antibodies or phalloidin. Figure 4 shows image sets observed at the lamellae, obtained using E-SPM and CLSM. In the images obtained using E-SPM, we focused on SF-like cables (Fig. 4a), filamentous networks (Fig. 4c), and microgranules (Fig. 4e). Along the SF-like cables, F-actin and myosin-IIA were observed (Fig. 4a, b). This

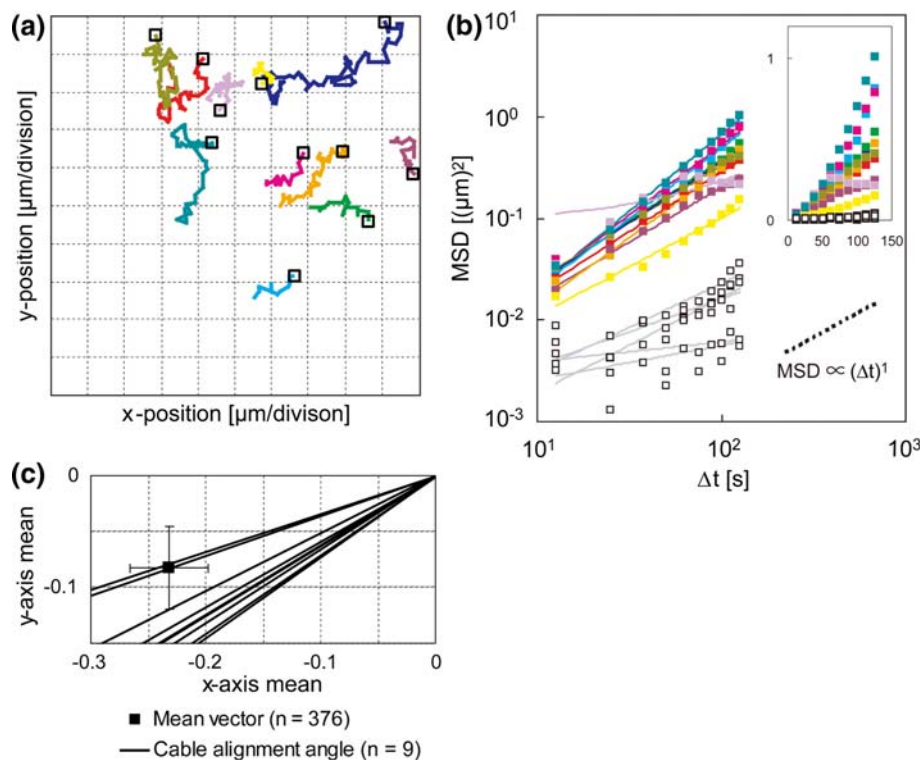


Fig. 3 Statistical analysis of microgranular movement. **a** Trajectories of the microgranules shown in Fig. 2 (polygonal lines). The colors distinguish 11 different microgranules. Starting positions of the trajectories are indicated by open squares. **b** MSD of the microgranules (solid symbols) and drift (open symbols) plotted as a function of time interval Δt in a double logarithmic fashion. The solid lines indicate power-law regressions. *Inset* identical MSD– Δt relationships

indicated that the cables were SFs. F-actin was observed in the filamentous networks but α -tubulin was not (Fig. 4c, d). These results indicated that the filamentous networks mainly comprised F-actin and not microtubules. We also found that some microgranules included F-actin and/or vinculin (Fig. 4e, f). Vinculin is known to be one of the general components of focal adhesions located at the ends of SFs. However, the vinculin foci at the microgranules did not associate with the SFs. This result implied that the vinculin foci were likely to be precursors of focal adhesions (Rottner et al. 1999). We noted that all the microgranules did not always include F-actin and vinculin, which meant that microgranules were not identical to the cytoskeleton or focal complexes. Microgranules might change their molecular compositions dynamically or be associated with various existing components in cells.

Drug-induced changes in mechanical architecture

To test the hypothesis that the filamentous architecture, including cables and thin filaments, is based on F-actin, we subjected the cells to pharmacological treatment during SP microscopic observation and examined the deconstruction

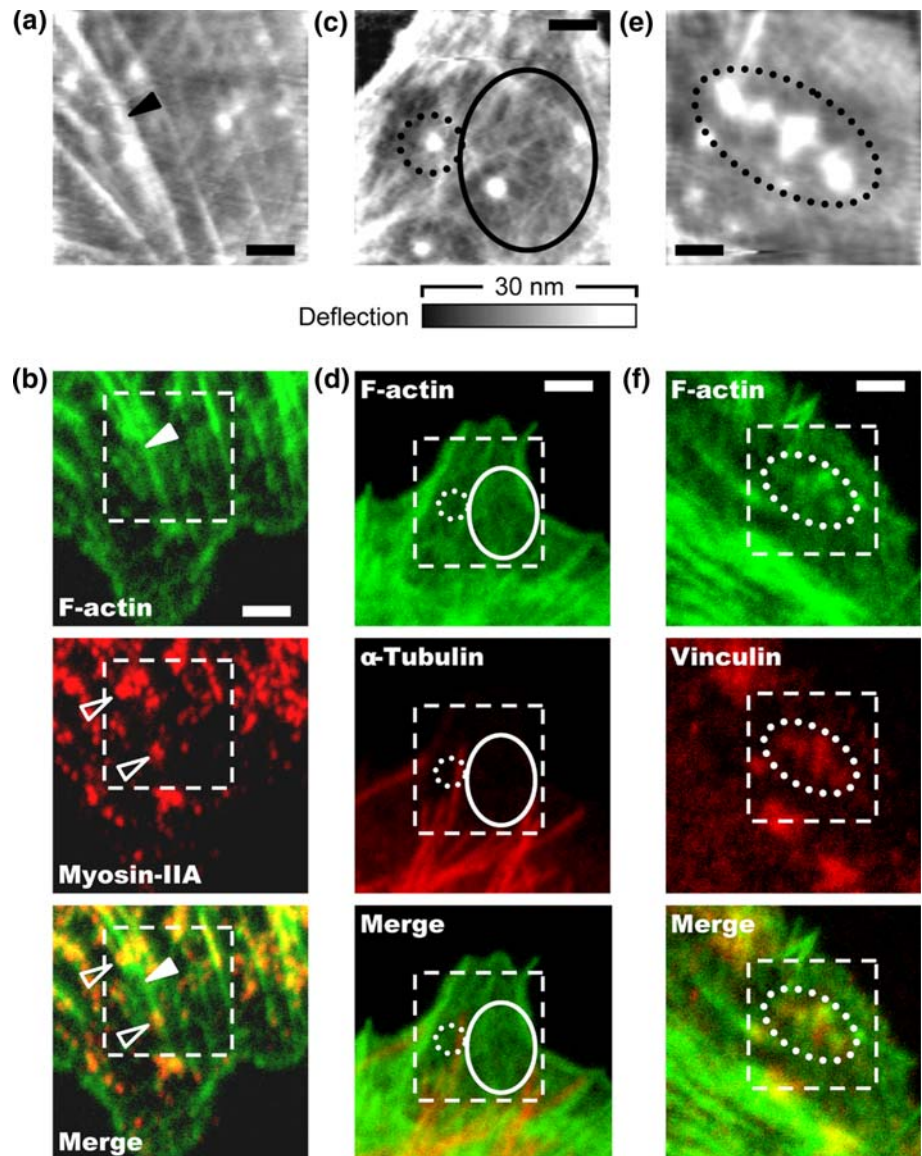
represented in a double linear fashion. The colors indicate microgranules corresponding to those shown in a. **c** Mean vector \mathbf{r} of 376 unitized displacement vectors, $\mathbf{u}_i(j)$, plotted on an x – y plane (solid square). The error bars indicate SE. The directional order, $|\mathbf{r}|$, is significantly different from 0, tested by Rayleigh's z test ($P < 0.001$). Solid lines indicate the alignment angles of the SF-like cables observed at 630 s

dynamics of filamentous architecture. First, we treated the cells with cytochalasin-D (Fig. 5a). The filamentous architecture, including the thick cables and thin filaments, immediately disappeared within 1 min after treatment. This indicated that the filamentous architecture depended on F-actin. Next, to determine whether the cables are SFs, we treated the cells with Y-27632, which disrupts SFs but not F-actin networks (Fig. 5b). Unlike cytochalasin-D, Y-27632 was required for >1 min to deconstruct the filamentous architecture. The cables gradually thinned with time and finally disappeared within 10 min after the treatment. However, thin filaments were still visible for 15 min after the treatment. This suggests that Y-27632 selectively digested the cables but not the thin filaments. Hence, we conclude that the cables visualized by SPM are in fact SFs.

Discussion

We believe that the high-speed live-cell SPM has great potential to investigate biological dynamics based on the structural changes in mechanical architecture. SPM allows visualization of mechanical architecture in a molecularly

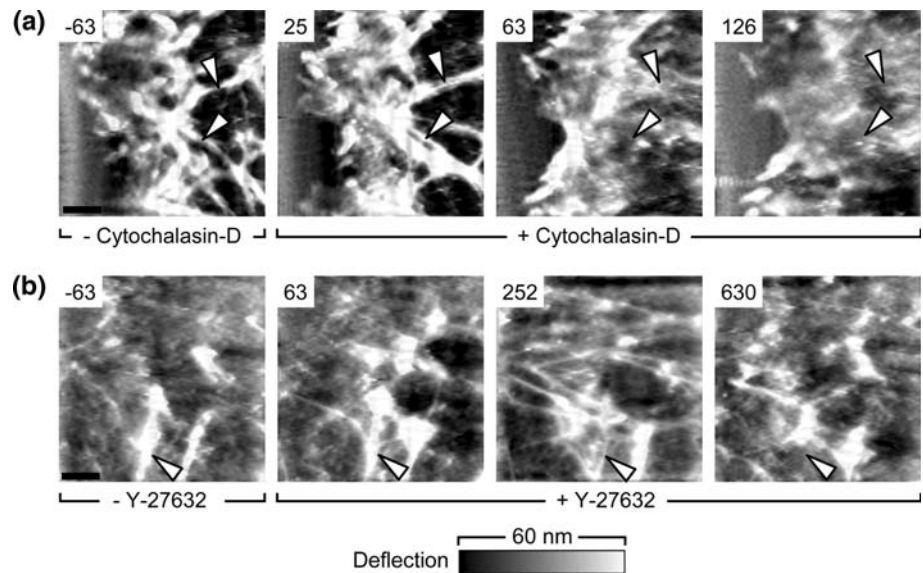
Fig. 4 Fluorescence microscopic analysis of the cables, networks, and microgranules visualized using E-SPM. **a, c, e** Images of lamellae of living fibroblasts obtained using E-SPM. The *solid arrowhead*, *solid ellipse*, and *dotted ellipses* indicate a cable, networks, and microgranules, respectively. **b** Distributions of F-actin and myosin-IIA visualized using CLSM in the cell shown in **a**. The *solid arrowheads* indicate the cable corresponding to the one in **a**, and the *open arrowheads* indicate myosin-IIA foci clearly localized at the F-actin cable. **d** Distributions of F-actin and α -tubulin visualized using CLSM in the cell shown in **c**. The *solid ellipses* indicate the area corresponding to the one indicated by the *solid ellipse* in **c**. **f** Distributions of F-actin and vinculin visualized using CLSM in the cell shown in **e**. The *dotted ellipses* indicate the area corresponding to the one indicated by the *dotted ellipse* in **e**. All *dashed squares* in the images obtained using CLSM correspond to the scan area on E-SPM. Scale bars 1 μm (**a, c, e**) and 2 μm (**b, d, f**)



nonspecific manner, whereas live-cell fluorescence microscopy, which is generally used to measure the spatial distribution and activation state of molecules in cells, allows visualization of only a couple of specific molecules. Recently, it has been suggested that the mechanical properties of cells are not based only on the actin cytoskeleton (Treat et al. 2007). Moreover, nonfilamentous microgranules have been visualized in various types of cells using contact-mode SPM (Schoenenberger and Hoh 1994; Le Grimellec et al. 1998; Yamane et al. 1999; Grzywa et al. 2006), but their molecular compositions were largely unknown. Therefore, an SP microscope that permits molecularly nonspecific microscopy and high-speed observation is required for investigating the dynamics of mechanical architecture. Previous types of high-speed SP microscopes, which are equipped with an ultrafast feedback

system or ultrafast oscillatory scanner, are quite effective for relatively stiff and small (submicrometer scale) samples but seem to be difficult to use for observing soft or large (micrometer scale) samples. In this study, we improved the temporal resolution in SPM for live-cell observation by introducing simple methods and achieved high-speed observation of the mechanical architecture in leading lamellae. Our data enabled analysis of the spatiotemporal dynamics at subminute temporal resolution. This temporal resolution is likely suitable to examine biological dynamics of not only leading lamellae but also other materials, such as epithelial microvilli (Gorelik et al. 2003). Our methods are only based on the commercial SPM system and the set of parameters for the system. The parameter set includes integral gain, proportional gain, and scan rate, which are the general parameters for SPM. Hence, we consider that our

Fig. 5 Drug-induced changes in mechanical architecture observed using time-lapse E-SPM. **a** Time-lapse images of the lamella of a living fibroblast treated with cytochalasin-D. **b** Time-lapse images of the lamella of a living fibroblast treated with Y-27632. The number in each image represents the time in seconds. The drug was added at time zero. The arrowheads indicate the positions of the SF-like cables that are visible before treatment. Scale bars 2 μ m



methods are easily and generally applicable to commercial SPM. However, temporal resolution is still limited to the subminute scale. Further improvement in the temporal resolution for live-cell E-SPM imaging may require special equipment(s) such as softer cantilevers for reducing cell damage and stable scanners for reducing image noise.

Superdiffusive movement of microgranules and its directional order suggest that non-Brownian processes drive the microgranules. It has been reported that microbeads linked to transmembrane protein integrin on cell surfaces show superdiffusion depending on actomyosin contractility in the time scale comparable to the microgranules (Bursac et al. 2005). Integrin colocalizes with vinculin, which is able to bind to actin directly (Menkel et al. 1994) or another actin-binding protein (McGregor et al. 1994), to connect to the actin cytoskeleton. Localization of vinculin at microgranules suggests that microgranules are associated with both integrin and the actin cytoskeleton for actomyosin-dependent superdiffusion. Further, the microgranules moved toward the cell body with a significant directional order. In lamellae, many intracellular components such as actin-related molecules show cell body-directed movement, called “retrograde flow” and driven by centripetal movement of actin cytoskeletal networks based on actomyosin contractility (Waterman-Storer and Salmon 1997; Ponti et al. 2004; Vallotton et al. 2004; Brown et al. 2006; Cai et al. 2006; Hu et al. 2007). Therefore, actomyosin contractility likely drives microgranules.

Although the biological function of microgranules in cells is unknown, the dynamical behaviors of microgranules may reflect their function. We found that the microgranular movement was oriented in the same direction as the alignment of newly formed SFs. We also found

that the number of microgranules decreased with the development of the SFs. Therefore, the dynamical behaviors of microgranules are possibly related to SF assembly. It has been reported that actomyosin contractility delivers F-actin for assembly of F-actin cables (Anderson et al. 2008), which elongate in the direction of the contractility (Hirata et al. 2007). As microgranules are likely delivered by actomyosin contractility and store F-actin occasionally, we speculate that microgranules transport F-actin and/or actin-binding proteins (e.g., vinculin) to assemble SFs. We will perform further experimental analysis to clarify the function of microgranules.

Acknowledgments We are grateful to Dr. Masayuki Takahashi (Division of Chemistry, Graduate School of Science, Hokkaido University, Sapporo, Japan) for the gift of anti-myosin-IIA antibody. We thank Dr. Koji Nemoto (Division of Physics, Graduate School of Science, Hokkaido University, Sapporo, Japan) for the valuable discussions. This study was supported by Grants-in-Aid for Exploratory Research (21654058) to K. K., Scientific Research (C) (21570158) to H. H., and JSPS Fellows (20.4710) to K. T. from the Ministry of Education, Culture, Sports, Science and Technology, Japan.

References

- Alcaraz J, Buscemi L, Grabulosa M, Trepast X, Fabry B, Farré R, Navajas D (2003) Microrheology of human lung epithelial cells measured by atomic force microscopy. *Biophys J* 84:2071–2079
- Anderson TW, Vaughan AN, Cramer LP (2008) Retrograde flow and myosin II activity within the leading cell edge deliver F-actin to the lamella to seed the formation of graded polarity actomyosin II filament bundles in migrating fibroblasts. *Mol Biol Cell* 19:5006–5018
- Ando T, Kodera N, Takai E, Maruyama D, Saito K, Toda A (2001) A high-speed atomic force microscope for studying biological macromolecules. *Proc Natl Acad Sci USA* 98:12468–12472

- Baumgartner W, Hinterdorfer P, Ness W, Raab A, Vestweber D, Schindler H, Dreckhahn D (2000) Cadherin interaction probed by atomic force microscopy. *Proc Natl Acad Sci USA* 97:4005–4010
- Benoit M, Gabriel D, Gerisch G, Gaub HE (2000) Discrete interactions in cell adhesion measured by single-molecule force spectroscopy. *Nat Cell Biol* 2:313–317
- Brown CM, Hebert B, Kolin DL, Zareno J, Whitmore L, Horwitz AR, Wiseman PW (2006) Probing the integrin-actin linkage using high-resolution protein velocity mapping. *J Cell Sci* 119:5204–5214
- Bursac P, Lenormand G, Fabry B, Oliver M, Weitz DA, Viasnoff V, Butler JP, Fredberg JJ (2005) Cytoskeletal remodelling and slow dynamics in the living cell. *Nat Mater* 4:557–561
- Cai Y, Biais N, Giannone G, Tanase M, Jiang G, Hofman JM, Wiggins CH, Silberzan P, Buguin A, Ladoux B, Sheetz MP (2006) Nonmuscle myosin IIA-dependent force inhibits cell spreading and drives F-actin flow. *Biophys J* 91:3907–3920
- Goffin JM, Pittet P, Csucs G, Lussi JW, Meister J-J, Hinz B (2006) Focal adhesion size controls tension-dependent recruitment of α -smooth muscle actin to stress fibers. *J Cell Biol* 172:259–268
- Gorelik J, Shevchuk AI, Frolenkov GI, Diakonov IA, Lab MJ, Kros CJ, Richardson GP, Vodyanoy I, Edwards CR, Klenerman D, Korchev YE (2003) Dynamic assembly of surface structures in living cells. *Proc Natl Acad Sci USA* 100:5819–5822
- Greenwood JA, Durand D (1955) The distribution of length and components of the sum of n random unit vectors. *Ann Math Stat* 26:233–246
- Grzywa EL, Lee AC, Lee GU, Suter DM (2006) High-resolution analysis of neuronal growth cone morphology by comparative atomic force and optical microscopy. *J Neurobiol* 66:1529–1543
- Habelitz S, Balooch M, Marshall SJ, Balooch G, Marshall GW Jr (2002) In situ atomic force microscopy of partially demineralized human dentin collagen fibrils. *J Struct Biol* 138:227–236
- Haga H, Sasaki S, Kawabata K, Ito E, Ushiki T, Sambongi T (2000) Elasticity mapping of living fibroblasts by AFM and immunofluorescence observation of the cytoskeleton. *Ultramicroscopy* 82:253–258
- Hansma PK, Schitter G, Fantner GE, Prater C (2006) High-speed atomic force microscopy. *Science* 314:601–602
- Helenius J, Heisenberg C-P, Gaub HE, Müller DJ (2008) Single-cell force spectroscopy. *J Cell Sci* 121:1785–1791
- Henderson E, Haydon PG, Sakaguchi DS (1992) Actin filament dynamics in living glial cells imaged by atomic force microscopy. *Science* 257:1944–1946
- Hertz H (1882) Über die berührung fester elastischer körper. *J Reine Angew Math* 92:156–171
- Hirata H, Tatsumi H, Sokabe M (2007) Dynamics of actin filaments during tension-dependent formation of actin bundles. *Biochim Biophys Acta* 1770:1115–1127
- Hu K, Ji L, Applegate KT, Danuser G, Waterman-Storer CM (2007) Differential transmission of actin motion within focal adhesions. *Science* 315:111–115
- Le Grimellec C, Lesniewska E, Giocondi MC, Finot E, Vié V, Goudonnet JP (1998) Imaging of the surface of living cells by low-force contact-mode atomic force microscopy. *Biophys J* 75:695–703
- Levenberg K (1944) A method for the solution of certain nonlinear problems in least squares. *Q Appl Math* 2:164–168
- Marquardt D (1963) An algorithm for least-squares estimation of nonlinear parameters. *J Appl Math* 11:431–441
- McGregor A, Blanchard AD, Rowe AJ, Critchley DR (1994) Identification of the vinculin-binding site in the cytoskeletal protein alpha-actinin. *Biochem J* 301:225–233
- Menkel AR, Kroemker M, Bubeck P, Ronsiek M, Nikolai G, Jockusch BM (1994) Characterization of an F-actin-binding domain in the cytoskeletal protein vinculin. *J Cell Biol* 126:1231–1240
- Pesen D, Hoh JH (2005) Micromechanical architecture of the endothelial cell cortex. *Biophys J* 88:670–679
- Picco LM, Bozec L, Ulcinas A, Engledew DJ, Antognozzi M, Horton MA, Miles MJ (2007) Breaking the speed limit with atomic force microscopy. *Nanotechnology* 18:044030
- Picco LM, Dunton PG, Ulcinas A, Engledew DJ, Hoshi O, Ushiki T, Miles MJ (2008) High-speed AFM of human chromosomes in liquid. *Nanotechnology* 19:384018
- Ponti A, Machacek M, Gupton SL, Waterman-Storer CM, Danuser G (2004) Two distinct actin networks drive the protrusion of migrating cells. *Science* 305:1782–1786
- Radmacher M, Fritz M, Kacher CM, Cleveland JP, Hansma PK (1996) Measuring the viscoelastic properties of human platelets with the atomic force microscope. *Biophys J* 70:556–567
- Raspanti M, Congiu T, Guizzardi S (2001) Tapping-mode atomic force microscopy in fluid of hydrated extracellular matrix. *Matrix Biol* 20:601–604
- Rottner K, Hall A, Small JV (1999) Interplay between Rac and Rho in the control of substrate contact dynamics. *Curr Biol* 9:640–648
- Schoenberger CA, Hoh JH (1994) Slow cellular dynamics in MDCK and R5 cells monitored by time-lapse atomic force microscopy. *Biophys J* 67:929–936
- Tamura K, Mizutani T, Haga H, Kawabata K (2007) Visualization of stretch-induced intracellular tensional response of single fibroblasts by mechanical scanning probe microscopy. *Jpn J Appl Phys* 46:5631–5635
- Trepats X, Deng L, An SS, Navajas D, Tschumperlin DJ, Gerthoffer WT, Butler JP, Fredberg JJ (2007) Universal physical responses to stretch in the living cell. *Nature* 447:592–595
- Vallotton P, Gupton SL, Waterman-Storer CM, Danuser G (2004) Simultaneous mapping of filamentous actin flow and turnover in migrating cells by quantitative fluorescent speckle microscopy. *Proc Natl Acad Sci USA* 101:9660–9665
- Waterman-Storer CM, Salmon ED (1997) Actomyosin-based retrograde flow of microtubules in the lamella of migrating epithelial cells influences microtubule dynamic instability and turnover and is associated with microtubule breakage and treadmilling. *J Cell Biol* 139:417–434
- Yamane Y, Shiga H, Asou H, Haga H, Kawabata K, Abe K, Ito E (1999) Dynamics of astrocyte adhesion as analyzed by a combination of atomic force microscopy and immunocytochemistry: the involvement of actin filaments and connexin 43 in the early stage of adhesion. *Arch Histol Cytol* 62:355–361
- Zar JH (1999) *Biostatistical analysis*. Prentice-Hall, Upper Saddle River